Journal of Applied Polymer Science

Polypyrrole Film Architectures Influence on Platinum Nanoparticles Efficiency in Ethanol Electrooxidation

Andrei Bogdan Stoian, George-Octavian Buica, Ioana Demetrescu
Department of General Chemistry, University POLITEHNICA of Bucharest, 011061 Bucharest, Romania
Correspondence to: I. Demetrescu (E-mail: i_demetrescu@chim.upb.ro)

ABSTRACT: The electrodeposition of polypyrrole films from aqueous surfactant solution through a two-dimensional polystyrene template onto indium-tin oxide substrate has been investigated. The polymer grows in the interstitial spaces of the self-assembled polystyrene spheres, which were subsequently removed by dissolution in toluene. The new obtained surface was characterized by scanning electron microscopy and atomic force microscopy. Platinum nanoparticles were deposited onto the nanostructured polypyrrole electrode and used as a catalyst for the oxidation of ethanol for direct ethanol fuel cells. © 2014 Wiley Periodicals, Inc. J. Appl. Polym. Sci. **2015**, *132*, 41375.

KEYWORDS: batteries and fuel cells; conducting polymers; nanoparticles; nanostructured polymers; nanowires and nanocrystals

Received 17 March 2014; accepted 6 August 2014
DOI: 10.1002/app.41375

INTRODUCTION

During the last decade, the trend of using more ecological friendly fuels and replacing classical fossil fuels with alternative sources of energy led to the development of a series of devices that are becoming increasingly popular. One of these devices is the direct ethanol fuel cell (DEFC), which is used mainly to power vehicles and electronic devices. The DEFCs have the advantages to produce low quantity pollutant emissions and to have high energy conversion efficiency. The advantage of using ethanol instead of methanol in fuel cells is due to the low toxicity of ethanol, easier production and higher energy density (8.00 kW h kg^{-1} for ethanol vs. 6.09 kW h kg^{-1} for methanol).[1–6]

Platinum is often used as a catalyst in these devices, usually in combination with other metals, which show catalytic effects for alcoholic oxidation process.[7–12] There is however an impediment: the price of obtaining these metals.[13] Thus, the present study aims to prove that by using dispersed nanoparticles of platinum in a film of conductive polymer deposited on the electrode surface instead of using a larger single piece, the obtained results would be comparable.

Since their discovery, conductive polymers have shown great advantages over other materials due to their high stability and ease of processing.[12,14–17] Electropolymerization is considered one of the most efficient routes for the synthesis of conductive polymers. One attractive procedure towards producing nanostructured conductive polymers is the employment of easily removable templates.[18,19]

As can be seen from literature, methanol fuel cells have been intensively investigated trying to improve the activity of the Pt-based catalysts, which have as demerit low catalytic activity, slow kinetics of methanol oxidation, and poor electrochemical stability. It is the toxic effect of carbon monoxide, which leads to the need of a better performance of the Pt catalysts. During the last decade various investigations have been done in order to solve such problems by the introduction of nanosized alloy catalysts[20] and the electrochemical elaboration of mono, bi, and trimetallic composites deposited on advanced carbon systems.[21,22] In this approach of Pt electrodeposition using various graphene structures, good results have been reached recently.[23] Of course the idea of using materials at nanoscale in fabrication of electrocatalysts has induced a better control in surface to volume ratio and the effect of nanodimensions was even more exploited by using as support for catalysts conductive polymer films such as polypyrrole with porous structures.[24] The influence of the electrocatalysts used in fuel cells fabrication, structure, and electroactivity has remained a subject, which needs to be studied[25] especially for electrooxidation of ethanol, which was much less investigated.

In the context of using a matrix of conductive polymers for the electrodeposition of Pt nanoparticles, the present article proposes a new method of electrodeposition of PPy films, growing them on a layer of PS spheres, which will enhance electrocatalyst area for ethanol oxidation. This is the aim and in the same time the novelty of this study, which improves the catalyst properties building a new kind of nanocomposite with complex hybrid nanoarhitecture.

The topography and morphology of the films were investigated with atomic force microscopy (AFM) and scanning electron microscopy (SEM). Electrochemical tests were performed to investigate how the architecture[26–30] of the electrode's surface affects the catalytic effect of the films in alcoholic oxidation.

EXPERIMENTAL

Materials and Reagents

Polystyrene nanospheres with diameters of 100 nm (Alfa Aesar 2.5 wt %) were further diluted with ultrapure water obtained from a Millipore Direct Q UV distiller until a concentration of 1.5 wt % was reached.

Ethanol and acetone 98% purity from Chimreactiv were used to clean the ITO glass electrodes and glassware.

Aqueous solutions with different concentrations (10^{-6} M, 10^{-5} M, and 10^{-4} M) of Triton X-100 (Sigma-Aldrich) were used as a post cleaning treatment of ITO glass electrodes.

Polypyrrole was electropolymerized from an aqueous solution of 50 m*M* pyrrole, 5 m*M* $LiClO_4$, and 30 m*M* Sodium dodecyl sulfate (SDS) all purchased from Sigma-Aldrich with purities ≥98%.

Platinum nanoparticles were electrodeposited from an aqueous solution of 25 m*M* H_2PtCl_6 (Sigma-Aldrich 38% Pt).

Electrochemical tests were performed in aqueous solutions of Ethanol 2*M*/H_2SO_4 0.1*M*, and an acetonitrile solution containing 0.1*M* Ferrocene and 0.1*M* $LiClO_4$ all purchased from Sigma-Aldrich 98% purity.

Instrumentation

Ultrasonication procedures were carried out with a Transsonic TI-H-S ultrasonication bath. All electrochemical procedures were carried out at room temperature using a Metrohm/Eco Chemie Autolab PGSTAT 302N Potentiostat/Galvanostat using a standard three electrode system with platinum or ITO glass plates as working electrodes, a platinum counter electrode and a Ag/AgCl 3*M* KCl as reference electrode.

The dispersion of the PS nanospheres was evaluated with a Zeiss Scope A1 optical microscope, the topography and morphologies were carried out using an A.P.E Research A100-SGS AFM with a conductive module and a QUANTA INSPECT F with field emission gun scanning electron microscope with a resolution of 1.2 nm.

AFM topography and conductivity maps were processed with Gwyddion 2.34 open source software. Electrochemical data were acquired with Nova 10 and processed with Origin 8.5 softawares.

Procedures

The Platinum electrode was cleaned with Al_2O_3 powder to remove the existing oxide from the surface, then purified by successively ultrasonication in water, ethanol and acetone—10 min in each medium at 130 kHz.

ITO glass plates were degreased by successively ultrasonication in water, ethanol, and acetone (10 min in each medium at 130 kHz), treated with Triton X-100 and uniformly covered with PS nanospheres.

Polypyrrole was electropolymerized on ITO glass plates by applying a constant potential of 0.7 V for 10 s, to avoid completely covering of the PS nanospheres. After the PPy deposition the PS nanospheres were removed by immersion in toluene for 2 h. A second ITO electrode was built using unpatterned PPy using the same conditions as above but without employing the use of PS nanospheres to be compared with the first.

Platinum nanoparticles were electrodeposited from a solution of H_2PtCl_6 at a cathodic current density of 3.5×10^{-4} A cm^{-2} for 200 s using the same three electrode system described above.

The catalytic effect of Pt was evaluated by cyclic voltammetry (CV) between −0.3 and 1.2 V with a scan speed of 0.025 V/s and the real area of the Pt electrode was calculated employing Randles–Sevcik equation from CVs taken between −0.25 and 0.8 V with varying scan speeds between 0.025 and 0.5 V/s using the system described before.

Electrochemical impedance spectroscopy (EIS) characterization was carried out at OCP in a logarithmic distribution range between 100 KHz and 10 mHz.

Electrode Preparation

The ITO/PPy/Pt electrodes were prepared in similar conditions using the following steps:

E1

a. The clean ITO glass plates were treated with an aqueous solution Triton X-100 (concentration 10^{-5} M).
b. A single drop of polystyrene sphere latex (concentration 1.5%) was spread on the ITO substrate. The excess latex was removed after partial evaporation.
c. AFM images were performed in order to inspect the formation of the polystyrene nanosphere monolayer.
d. Polypyrrole was electropolymerized from an aqueous solution of 50 m*M* pyrrole, 5 m*M* $LiClO_4$, and 30 m*M* SDS using a potential of 0.7 V for 10 s with the nanospheres still in place.
e. AFM and SEM images were taken to verify if the PPy film was uniform and thin enough as not to disturb the nanosphere previous arrangement.
f. The polystyrene spheres were removed from the ITO/PPy electrode by immersion in toluene.
g. AFM and SEM micrographies were performed in order to investigate the formation of the template.
h. Platinum nanoparticles were electrochemically deposited from a solution of H_2PtCl_6 at a cathodic current density of 3.5×10^{-4} A cm^{-2} for 200 s.

E2

a. The clean ITO glass plates were treated with an aqueous solution Triton X-100 (concentration 10^{-5} M).
b. Polypyrrole was electropolymerized from an aqueous solution of 50 m*M* pyrrole, 5 m*M* $LiClO_4$, and 30 m*M* SDS using a potential of 0.7 V for 10 s.

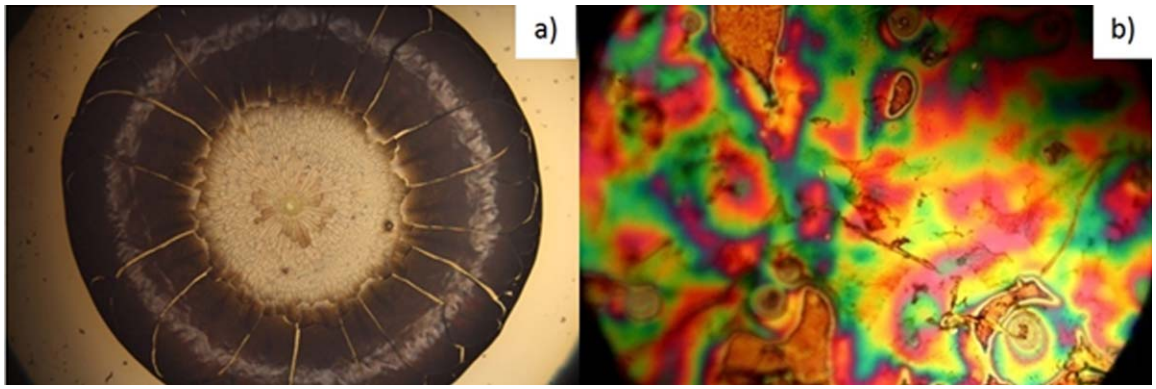

Figure 1. Optical micrograph (5× magnification) of polystyrene spheres on ITO without (a) Triton X-100 treatment and (b) including Triton X-100 treatment. [Color figure can be viewed in the online issue, which is available at wileyonlinelibrary.com.]

c. AFM images were taken to verify if the PPy film was uniform and composed of small grains.
d. Platinum nanoparticles were electrochemically deposited from a solution of H_2PtCl_6 at a cathodic current density of 3.5×10^{-4} A cm^{-2} for 200 s.

RESULTS AND DISCUSSION

The Effect of Triton X-100 Treatment on the Assembly of PS Nanospheres

After the degreasing procedure of an ITO glass piece, a single drop of PS nanosphere latex was placed on the surface. The surface forces were too high to permit the uniform covering and auto assembling of the spheres (Figure 1) and inhibited the formation of the desired monolayer. Figure 1(b) presents the optical micrograph after the treatment of an ITO glass piece with Triton X-100 and spheres immobilization.

Aqueous solutions with various concentrations of Triton X-100 (10^{-6} M, 10^{-5} M, and 10^{-4} M) were used to assess the optimal concentration of Triton X-100 needed for the desired result. AFM scans (Figure 2) revealed that either higher and lower concentrations than necessary of Triton X-100 inhibit the auto assembly of the polystyrene spheres as follows: a low concentration leads to multiple layers of spheres on the surface, while a high concentration results in a monolayer interrupted by large gaps present between the spheres.

The best results were given by a concentration of Triton X-100 of 10^{-5} M, which produced the monolayer with the desired architecture i.e. spheres close together forming a uniform covering of the electrode's surface and with no gaps present.

Coloidal particles are able to auto assemble to form templates by different methods, like centrifugation or evaporation. The template was assembled over the ITO substrate using Triton X-100. This amphiphilic nonionic surfactant is used to stabilize the polystyrene spheres. The interaction between the nonpolar part of the surfactant and the hydrophobic polystyrene latex surface leads to the formation of the template. The concentration of the used surfactant is dependent on the hydrophilic/hydrophobic characteristics of the substrate as well as the concentration of the used latex. Goncales et al. reported similar results in their work.[31]

Electropolymerization of Pyrrole

Initially PPy was electrodeposited without the addition of surfactants as in the method described in the electrode preparation section. It was observed via AFM imaging, that PPy formed large structures that pushed the nanospheres up and sideways [Figure 3(a, b)], breaking their order and prohibiting the formation of the desired template. The formation of these large structures was inhibited by adding SDS[32,33] in the polymerization solution. The addition of SDS to the polymerization solution enables the formation of micelles. The pyrrole monomer enters in the formed micelles due to its more hydrophobic properties. The polypyrrole particle size is inversely proportional with the concentration of the surfactant in the solution i.e. higher surfactant concentration leads to the formation of smaller polypyrrole particles. This result can be explained by the decreasing size of the micelles present when higher concentrations of surfactant are used.[34] Further improvements were made by varying the applied potential and time of the process. The best results [Figure 3(c)] were obtained using a potential of

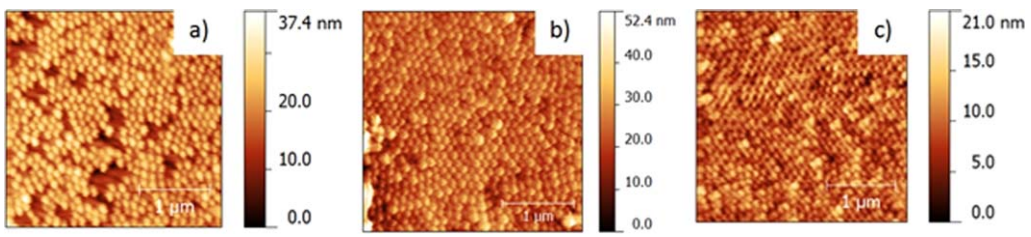

Figure 2. AFM topographies for polystyrene spheres after using a treatment with Triton X-100 (a) 10^{-4} M; (b) 10^{-5} M; and (c) 10^{-6} M. [Color figure can be viewed in the online issue, which is available at wileyonlinelibrary.com.]

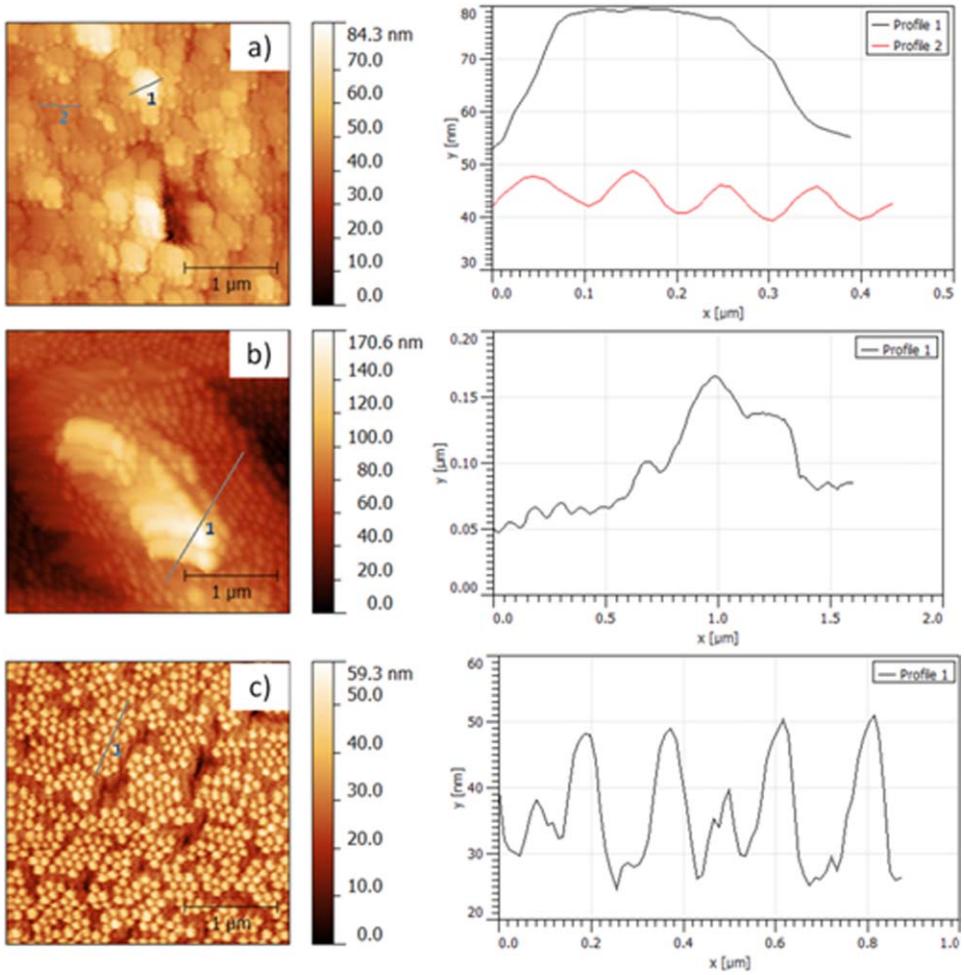

Figure 3. AFM topography images and linear profiles of polypyrrole structures (a) 0.7 V–10 s; (b) 0.8 V–10 s; (c) 0.7 V–10 s + SDS. [Color figure can be viewed in the online issue, which is available at wileyonlinelibrary.com.]

0.7 V for 10 s, which produced a PPy film with a height of about 70 nm. The thickness of the film enabled the formation of a template after removing the PS spheres.

The Polypyrrole Template

The PS nanospheres were removed from the surface by dipping the ITO/PPy electrode in toluene for 2 h. AFM and SEM images (Figure 4) revealed that the PPy film grew on ITO surface upwards and around the PS nanospheres, forming a matrix of hollow half spheres with the diameter of ~100 nm. This type of architecture enabled a growth in the real area of the ITO electrode and provided numerous nucleation sites for Pt nanoparticles, which were further uniformly distributed on the new surface.

Morphological Film Characterization

The morphology of the films was investigated by extracting linear profiles from the AFM scans. Film thickness was investigated by indenting the films and performing AFM scans in the section. The results (Figure 5) show that the two electrodes have very different morphologies and thicknesses. E1 is formed by the matrix of hollow half spheres with diameters of 90–100 nm formed after the removal of the PS spheres. The thickness of the film was an average height of 37 nm. E2 is formed by grains of PPy ranging in diameters between 120 nm and 1.5 µm. The thickness of the film was an average height of 65 nm.

The fact that the PPy films show different topographical characteristics can be explained by the electrochemical deposition phenomena that take place on the surface of the ITO glass electrodes. In the case of E1 the PPy film starts to grow in the spaces between the spheres and it's forced to form the template. This phenomenon does not take place on E2 since there are no spheres present on the surface, thus the PPy film forms freely, thus eventually reaching the classical cauliflower structures.

Fabrication of Electrodes

Platinum nanoparticles were electrodeposited from a solution of H_2PtCl_6 at an cathodic current density of 3.5×10^{-4} A cm^{-2} for 200 s on two PPy modified ITO glass plate in order to investigate the influence of the electrodes architecture and their efficiency.[35]

Electrochemical Characterization

The catalytic effect of the Pt nanoparticles was characterized by CV in an aqueous solution of Ethanol 2*M* and H_2SO_4 0.1*M* between −0.3 and 1.2 V with a scan rate of 0.025 V/s. The results obtained from a square piece of platinum with a

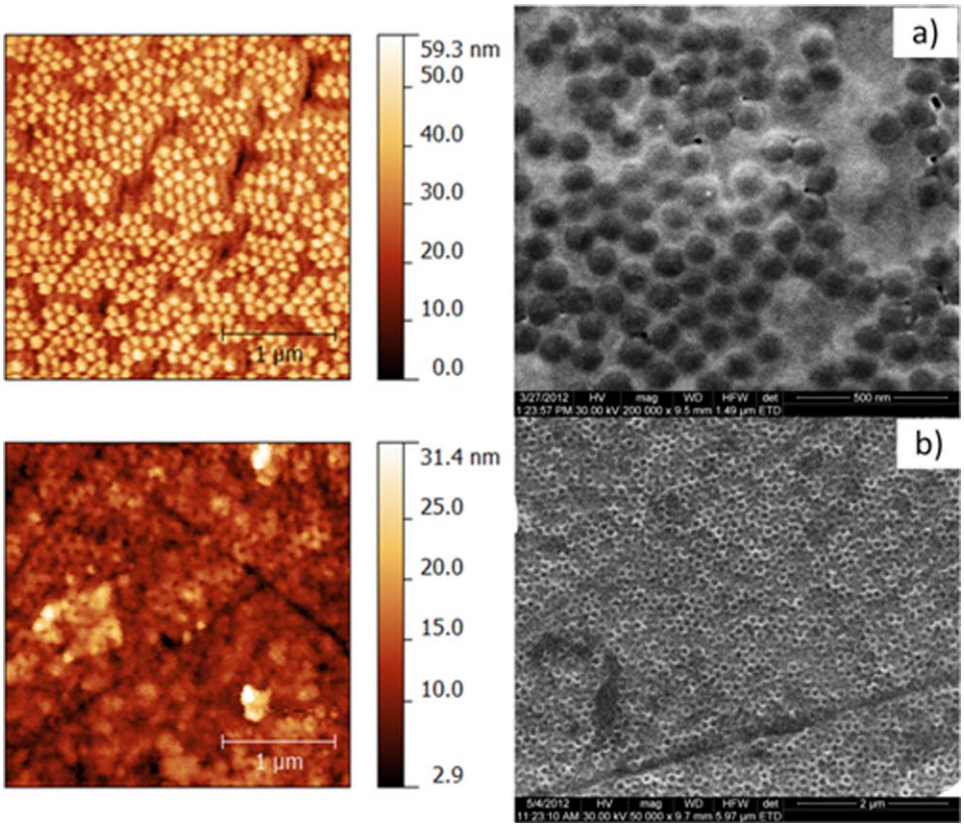

Figure 4. AFM (left) and SEM (right) micrographs of polypyrrole template on ITO glass (a) before PS spheres removal; (b) after PS spheres removal. [Color figure can be viewed in the online issue, which is available at wileyonlinelibrary.com.]

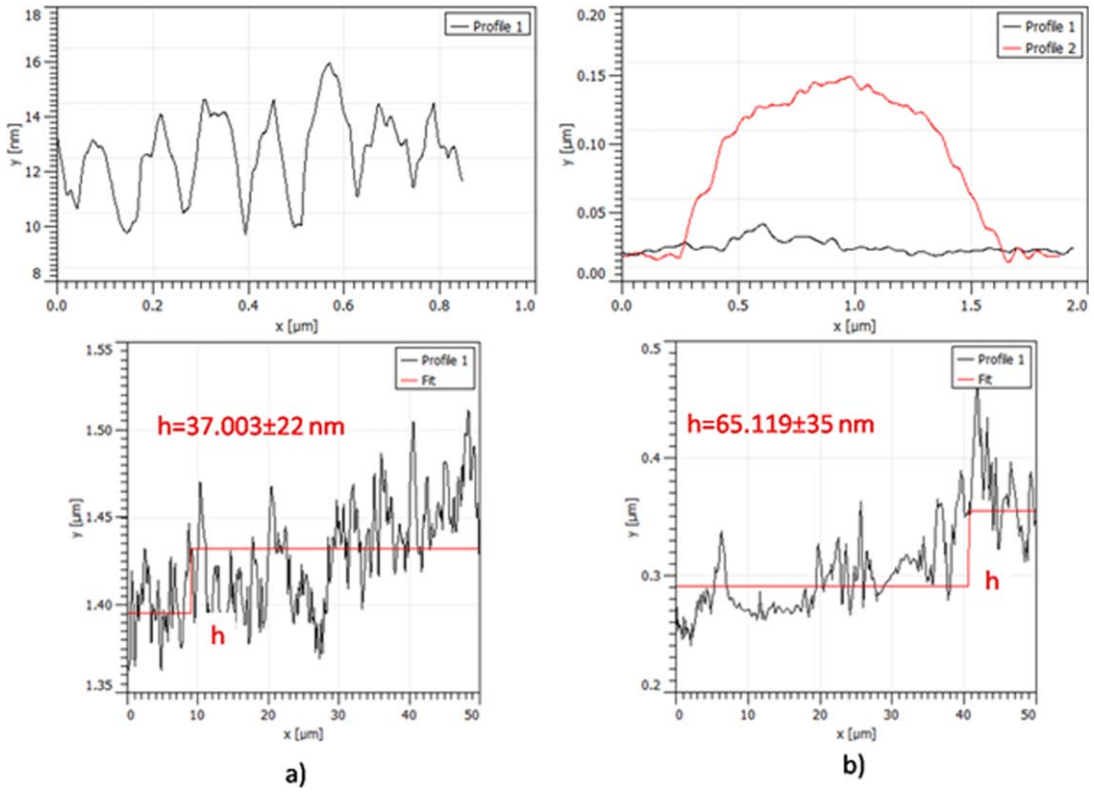

Figure 5. Linear profiles of (a) E1 and (b) E2. [Color figure can be viewed in the online issue, which is available at wileyonlinelibrary.com.]

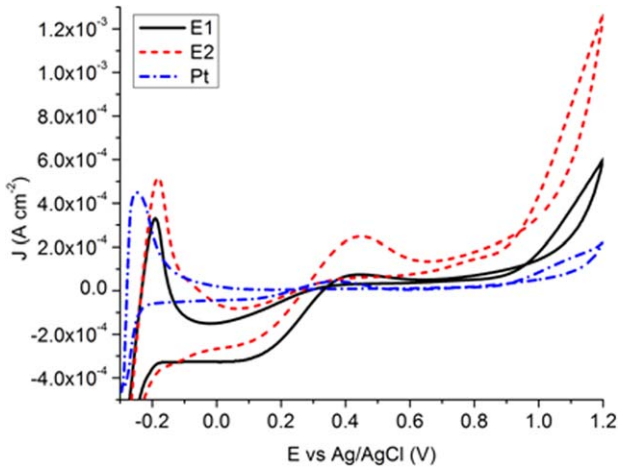

Figure 6. Cyclic voltamograms of E1, E2, and Pt in Ethanol 2*M*/H_2SO_4 0.1*M*. [Color figure can be viewed in the online issue, which is available at wileyonlinelibrary.com.]

projected geometric area of 12.5 cm^2 were used as reference for comparing the signals given by the ITO electrodes (4 cm^2).

All electrodes show peaks in the potential range from −0.3 to 0V (Figure 6). These cathodic peaks are specific to the adsorption of hydrogen.[36] The anodic peaks of the reverse scans around 0.4 V represent the reoxidation of the intermediate species produced in the forward scan.[37] The current density and total charge involved in the hydrogen adsorption/desorption region depend on the composition of the electrode and vary with the Pt loading. The integrated intensity of these peaks represents the number of Pt sites that are available for hydrogen adsorption and desorption.

The catalytic effect of E1 and E2 can be estimated by calculating the electrochemical active surface areas (EASA) from the charge associated to hydrogen desorption after correction of the double layer capacitive contribution. Assuming the formation of a hydrogen monolayer on the surface of platinum and the adsorption of one hydrogen atom per platinum atom, literature gives the electrical charge generally associated with monolayer adsorption of hydrogen value of 210 $\mu C\ cm^{-2}$.[38]

The experimentally obtained charges were calculated with the formula:

$$Q_H = \frac{1}{v}\int_{-0.3}^{-0.1} (I - I_d)\,dE \qquad (1)$$

where QH (C) is the charge, I (A) is the total current, I_d (A) the double layer current, E is the potential (V vs. Ag/AgCl) and v (V/s) the scan rate.

The electrochemical active surface area (EASA) S in cm^2 was determined as follows:

$$S = \frac{Q_H}{\theta_H \times 210 \mu C cm^{-2}} \qquad (2)$$

where Q_H is charge in μC, 210 μC cm^{-2} corresponds to a monolayer of adsorbed hydrogen and θ_H is the hydrogen monolayer coverage at end-point potential and is considered 1.

The real area of the Platinum electrode was calculated using Randles–Sevcik equation[39] from an Acetonitrile solution containing 0.1*M* Ferrocene and 0.1*M* $LiClO_4$ as supporting electrolyte.

$$I_P = 2.72\times10^5 \times n^{3/2} \times A \times D^{1/2} \times C \times v^{1/2} \qquad (3)$$

The results fitted well (Figure 7) and the calculated area of the Platinum electrode was found as 25.25 cm^2, two times as large as the geometrical area.

Table I summarizes the experimental data obtained for the two electrodes. It should be noted that the theoretical charge of 210 μC cm^{-2} represents an ideal case of an ultra-smooth electrode surface for which the geometric value is the same as the real value. In our case the large uneven surface of the Pt electrode leads to the existence of more adsorption sites on the surface. Although all electrodes show similar electrochemical activities in hydrogen adsorbtion/desorbtion processes, the best results in ethanol oxidation represented in the anodic peak of the reverse scans around 0.4 V were given by E2.

This surprising fact can be attributed to the morphology of the resulted PPy films. Platinum nucleation sites form in the defects of the polymeric films. Because of the employment of PS spheres in the fabrication of E1, the resulted PPy film was thinner and more compact than the one formed on E2. This fact allowed the Pt particles to assemble differently on the two electrodes. On E1, the Pt nanoparticles were smaller and uniformly dispersed on the surface, whereas on E2, Platinum formed larger structures, partly embedded in the film.

Electrode Stability Evaluation

The modified electrodes stabilities were evaluated by CV and EIS characterizations for 100 h, storing the electrodes immersed in ethanol between experiments to simulate continuous use.

Figure 8 shows the evolution of the cyclic voltammograms for E1 and E2. Both electrodes show similar behavior during the experiments. Although the hydrogen peaks are larger for E2, overall hydrogen evolution is better for E1. This can be attributed to the fact that on E1 Pt particles are more exposed to the electrolyte solution than on E2. The peaks associated with acetaldehyde formation and water decomposition are larger for E2 as well as the peaks associated with the reoxidation of intermediate species. The intermediate species are hard to oxidize at low potentials and cause catalyst contamination. In the backward scan, the reduction of oxide species allows the reoxidation of ethanol and intermediate species. Taking this in consideration, we can sustain that for E1, the Pt catalyst is more susceptible to contamination than on E2, in the latter case, a good

Table I. Experimental Values Obtained for Pt and ITO-PPy-Pt Electrodes

Electrode	Projected geometric area (cm^2)	Area calculated by AFM (cm^2)	EASA calculated by CV ($cm^2\ cm^{-2}$)	Q_H (μC cm^{-2})
Platinum	12.5	16.5	1.57	331
E1	4	4.04	1.36	286
E2	4	4.3	1.49	314

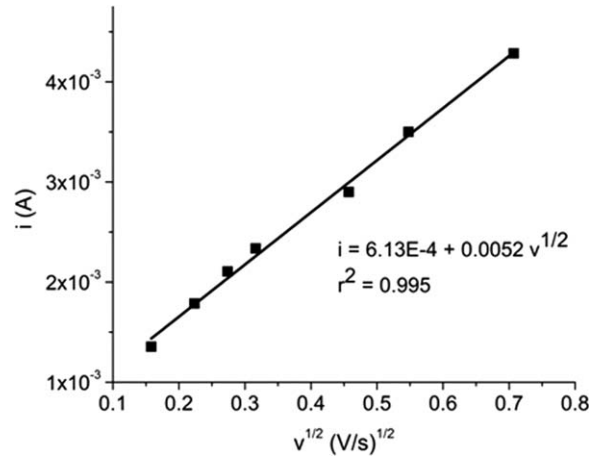

Figure 7. Randles–Sevcik plot of peak current vs. square root of the scan rate for platinum electrode.

portion of the platinum structure being protected by the PPy film. However, due to the fact that PPy becomes more porous over time as a result of overoxidation, the resulted products of ethanol oxidation remain trapped in the film, which causes the overall degradation of the electrodes.

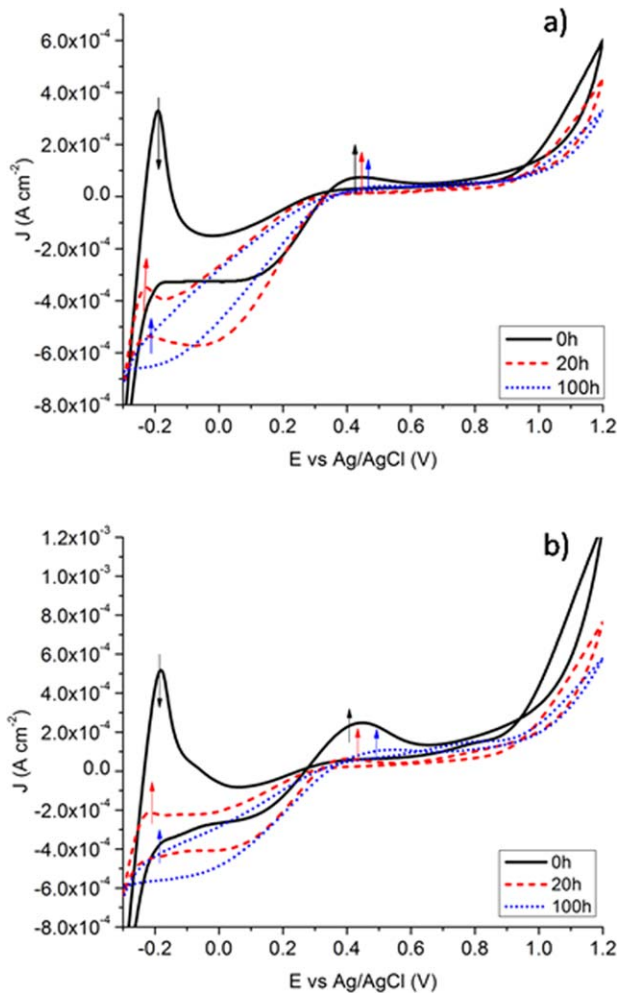

Figure 8. Cyclic voltamograms of (a) E1 and (b) E2 in ethanol 2*M*/H_2SO_4 0.1*M*. [Color figure can be viewed in the online issue, which is available at wileyonlinelibrary.com.]

Electrochemical impedance spectroscopy (EIS) characterization was carried out at OCP in a logarithmic distribution range between 100 KHz and 10 MHz. The overall impedance values were two times higher for E1 than for E2 and both electrodes showed similar evolution.

The data [Figure 9] were fitted by the equivalent circuit presented in Figure 10, where **Rs** represents the resistance of the electrolyte, **Rf** represents the resistance of the film and **tanh** represents a finite diffusion element used for thin films.

The results of the fitted experimental data are summarized in Table II. The resistance of E1 was around two times as large as for E2. The increase of the resistance with time is of about 60%, but is more accelerated for E2. The increase in resistance is due to the overoxidation of PPy during the electrochemical tests. The element **tanh** can be used to evaluate indirectly the thickness of the film. From the initial data we can conclude that E2 was thicker, this fact also being sustained by the AFM investigations. After 100 h, both films show similar values for this element. This can be attributed to the degradation of the PPy film, which produces a more porous film.

Conductivity Evaluation

A set of conductive AFM scans was performed on the three electrodes in order to investigate the differences observed by cyclic voltammetery. The resulting images give valuable information about the mechanisms of Pt electrodeposition on PPy. The colors on the conductivity maps represent highly conductive areas (white) dispersed in less conductive areas (black).

For the platinum electrode [Figure 11(a)] the topographic scan reveals a surface coated with dense rod-like oxide structures formed by spheres with a diameter of ~150 nm in spite of the pre-experiment preparations. The conductivity of this electrode is relatively homogenous, few less conductive surfaces being present on the surface.

On E2 [Figure 11(b)] classical cauliflower structures are present on the surface as expected. It seems that these structures provide less nucleation sites for platinum electrodeposition, since the conductive sites attributed to platinum are found only at the boundaries between the PPy structures. The sites containing platinum are long and narrow with lengths between 300 and 600 nm and widths of about 100 nm filling the interpolymeric spaces. This particular phenomenon explains the results given by the CV,

Table II. Electrical Parameters Resulted After Fitting the EIS Data for E1 and E2

Electrode	Element	0 h	20 h	100 h
E1	R_s [Ω]	15	26	58
	R_f [KΩ]	2.42	3.12	3.99
	tanh [$s^{1/2}$]	0.028	0.037	0.051
E2	R_s [Ω]	13	27	60
	R_f [KΩ]	1.1	1.72	1.88
	tanh [$s^{1/2}$]	0.035	0.041	0.053

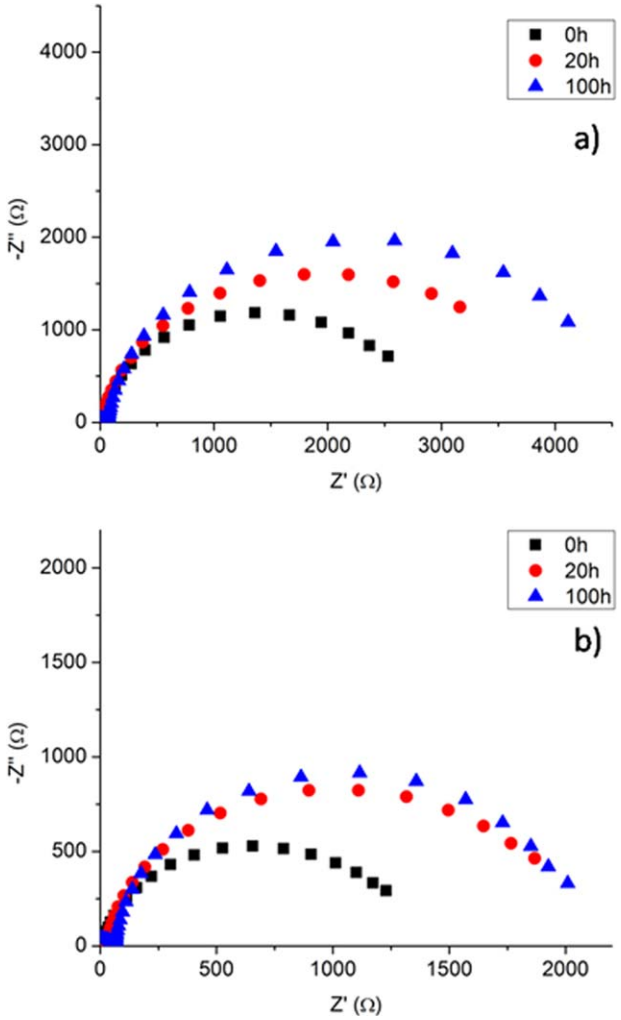

Figure 9. Nyquist plots of (a) E1 and (b) E2 in ethanol $2M/H_2SO_4$ $0.1M$ at OCP. [Color figure can be viewed in the online issue, which is available at wileyonlinelibrary.com.]

since platinum formed compact structures: only a small surface area of platinum was available for the catalytic processes and thus the small signal of the CV.

E1 [Figure 11(c)] is formed by hollow half spheres with more or less well defined ridges. Although not visible on the topography images due to their small size (20 nm or less) the platinum nanoparticles are well dispersed within the film. The good dispersion of the particles allows the maximization of the working area and thus produces a good catalytic effect, confirmed by the CV.

We can conclude that the electrodeposition of platinum on PPy is highly dependent on the architecture of the polymeric film, since for both electrodes the electrodeposition conditions were identical. The thinner and patterned PPy film may allow a greater efficiency for the electrodeposition of platinum by allowing a higher current efficiency and providing the many nucleation sites necessary for the nanoparticles of metal to adhere on the film.

Statistical Analysis

Statistical analysis calculated from AFM scans reveal that the surface area of the ITO-PPy electrodes was enlarged only in a small degree (1.2%) using the matrix formed by the PPy template (Figure 12, E1), and more (7,5%) for the electrode using cauliflower structured PPy (Figure 12, E2). The data show that the increase in area of the electrode by using the PS nanospheres of 100 nm in diameter is not as large as previously thought. Although the employment of the PS sphere template led to a better dispersion of the Pt nanoparticles, at this small scale a less dense PPy film seems to be desirable in order to permit the initial protection of Pt from the contaminants resulted during the oxidation of ethanol.

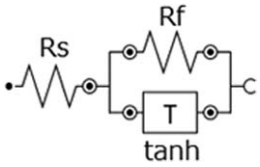

Figure 10. Equivalent ciruit for E1 and E2.

CONCLUSIONS

We have successfully obtained a monolayer of PS spheres on the surface of ITO glass, which has been used to create a template of hollow half spheres of Polypyrrole on the surface. Disperse platinum nanoparticles were electrodeposited on the surface of the PPy modified electrodes and electrochemically characterized. It has been found that the platinum nanoparticle electrodeposition

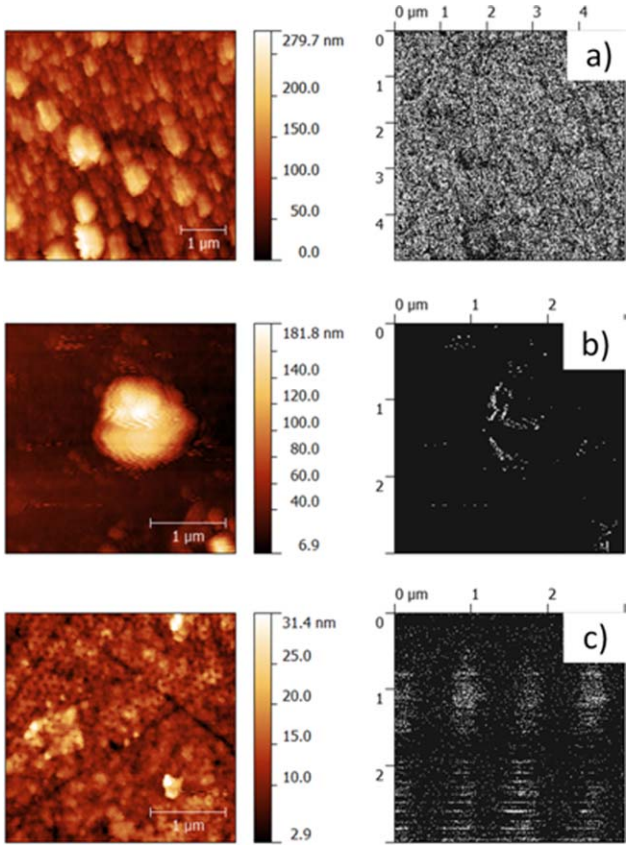

Figure 11. C-AFM scan images of (a) Platinum, (b) E2, and (c) E1 electrodes. [Color figure can be viewed in the online issue, which is available at wileyonlinelibrary.com.]

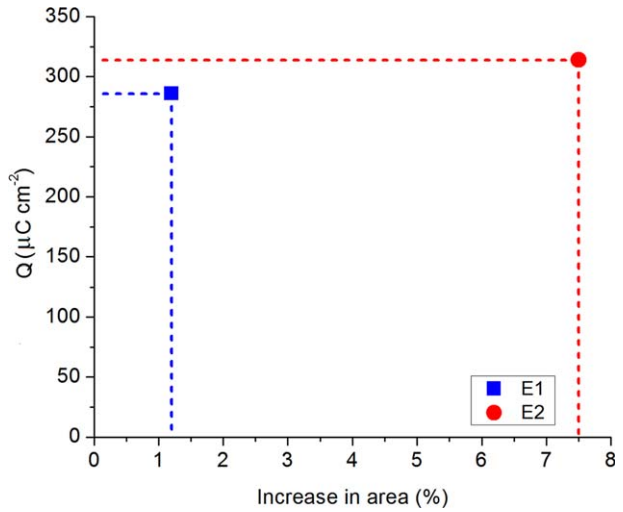

Figure 12. Statistical analysis of area increase and charge. [Color figure can be viewed in the online issue, which is available at wileyonlinelibrary.com.]

is highly dependent on the architecture of the PPy film. The electrochemical activities of both electrodes are comparable to that of the Platinum electrode. On the basis of these results, we can assume that using nanospheres with such small diameters (100 nm) does not influence greatly the electrochemical activity of the electrode, more studies being needed by employing spheres with larger diameters. However, we believe that this work could be a step could be useful as a step in building catalytic porous nanostructured membranes by removing the polymeric film from the substrate on which it was grown.

ACKNOWLEDGMENTS

Andrei Bogdan Stoian recognizes the financial support granted by the European Social Fund and the Romanian Government under the contract number POSDRU/159/1.5/S/137390/.

AUTHOR CONTRIBUTION

All authors had important contributions in the work related to this article. A.B. Stoian had the ideea of using PS nanospheres to create a templated PPy film with dispersed Pt nanoparticles, aquired and interpreted the topograph data and partly the electrochemical data and drafted part of the article. G.O. Buica provided the electrochemical cell setups, performed a part of the electrochemical testing and had a major role in interpretetion of the electrochemical data. He also had a role in devoloping the initial ideea and in drafting the article. I. Demetrescu had a major role in coordonating the others in all the stages of this work from the initial ideea in selecting the application of the experiment, to the interpretation of the data and critically revising the manuscript. All listed authors approve the submitted and final versions of this work.

REFERENCES

1. Ekdharmasuit, P.; Therdthianwong, A.; Therdthianwong, S. *Fuel.* **2013**, *113*, 69.
2. Friedl, J.; Stimming, U. *Electrochim. Acta.* **2013**, *101*, 41.
3. Kavanagh, R.; Cao, X. M.; Lin, W. F.; Hardacre, C.; Hu, P. *Angew. Chem. Int. Edit.* **2012**, *51*, 1572.
4. Kamarudin, M. Z. F.; Kamarudin, S. K.; Masdar, M. S.; Daud, W. R. W. *Int. J. Hydrogen Energy* **2013**, *38*, 9438.
5. Kobayashi, T.; Otomo, J.; Wen, C. J.; Takahashi, H. *J. Power Sources* **2003**, *124*, 34.
6. Tiwari, J. N.; Tiwari, R. N.; Singh, G.; Kim, K. S. *Nano Energy* **2013**, *2*, 553.
7. Saleh, F. S.; Easton, E. B. *J. Power Sources* **2014**, *246*, 392.
8. Pereira, A. O.; Miranda, C. R. *Appl. Surf. Sci.* **2014**, *288*, 564.
9. Kulesza, P. J.; Pieta, I. S.; Rutkowska, I. A.; Wadas, A.; Marks, D.; Klak, K.; Stobinski, L.; Cox, J. A. *Electrochim. Acta* **2013**, *110*, 474.
10. Zhang, G. R.; Ding, B. B.; Wu, L.; He, L.; Ni, B.; Lu, J. X. *J. Appl. Polym. Sci.* **2013**, *129*, 1593.
11. Jia, Y. J.; Jiang, J. C.; Sun, K.; Dai, T. Y. *J. Appl. Polym. Sci.* **2012**, *125*, 3702.
12. Ehsani, A.; Mahjani, M. G.; Jafarian, M.; Naeemy, A. *Electrochim. Acta* **2012**, *71*, 128.
13. Hasa, B.; Kalamaras, E.; Papaioannou, E. I.; Sygellou, L.; Katsaounis, A. *Int. J. Hydrogen Energ.* **2013**, *38*, 15395.
14. Pirvu, C.; Manole, C. C.; Stoian, A. B.; Demetrescu, I. *Electrochim Acta* **2011**, *56*, 9893.
15. Popescu, S.; Pirvu, C.; Mindroiu, M.; Demetrescu, I. *Mol. Cryst. Liq. Cryst.* **2010**, *522*, 425.
16. Pirvu, C.; Manole, C. C. *Electrochim. Acta* **2013**, *89*, 63.
17. Mindroiu, M.; Pirvu, C.; Popescu, S.; Demetrescu, I. *Mater. Plast.* **2009**, *46*, 394.
18. Li, C.; Bai, H.; Shi, G. Q. *Chem. Soc. Rev.* **2009**, *38*, 2397.
19. Wang, T. Q.; Zhong, W. B.; Ning, X. T.; Wang, Y. X.; Yang, W. T. *J. Appl. Polym. Sci.* **2009**, *114*, 3855.
20. Kim, K. J.; Kim, Y. H.; Jeong, W. J.; Jeong, S. W.; Park, J. C.; Ahn, H. G. *J. Nanosci. Nanotechnol.* **2007**, *7*, 4073.
21. Singh, B.; Murad, L.; Laffir, F.; Dickinson, C.; Dempsey, E. *Nanoscale* **2011**, *3*, 3334.
22. Hu, Y. J.; Zhang, H.; Wu, P.; Zhang, H.; Zhou, B.; Cai, C. X. *Phys. Chem. Chem. Phys.* **2011**, *13*, 4083.
23. Wang, X. L.; Li, C.; Shi, G. Q. *Phys. Chem. Chem. Phys.* **2014**, *16*, 10142.
24. Zhao, L.; Tong, L.; Li, C.; Gu, Z. Z.; Shi, G. Q. *J. Mater. Chem.* **2009**, *19*, 1653.
25. Coutanceau, C.; Brimaud, S.; Lamy, C.; Leger, J. M.; Dubau, L.; Rousseau, S.; Vigier, F. *Electrochim. Acta* **2008**, *53*, 6865.
26. Zhou, Y.; Hu, X. C.; Xiao, Y. J.; Shu, Q. *Electrochim. Acta* **2013**, *111*, 588.
27. Hua, H.; Hu, C. G.; Zhao, Z. H.; Liu, H.; Xie, X.; Xi, Y. *Electrochim. Acta* **2013**, *105*, 130.
28. Dai, L.; Jiang, L. P.; Abdel-Halim, E. S.; Zhu, J. J. *Electrochem. Commun.* **2011**, *13*, 1525.
29. Carmo, M.; Sekol, R. C.; Ding, S. Y.; Kumar, G.; Schroers, J.; Taylor, A. D. *Acs. Nano.* **2011**, *5*, 2979.

30. Ren, L.; Hui, K. S.; Hui, K. N. *J. Mater. Chem. A* **2013**, *1*, 5689.
31. Goncales, V. R.; Massafera, M. P.; Benedetti, T. M.; Moore, D. G.; de Torresi, S. I. C.; Torresi, R. M. *J. Brazil. Chem. Soc.* **2009**, *20*, 663.
32. Ma, Y. J.; Wang, H.; Ji, S.; Linkov, V.; Wang, R. F. *J. Power Sources* **2014**, *247*, 142.
33. Mindroiu, M.; Ion, R.; Pirvu, C.; Cimpean, A. *Mater. Sci. Eng. C: Mater.* **2013**, *33*, 3353.
34. Xing, S. X.; Zhao, G. K. *E-Polymers* **2007**, *7*, 202.
35. Ferreira, V. C.; Melato, A. I.; Silva, A. F.; Abrantes, L. M. *Electrochim. Acta* **2011**, *56*, 3567.
36. Frelink, T.; Visscher, W.; Vanveen, J. A. R. *Electrochim. Acta* **1995**, *40*, 545.
37. Razmi, H.; Habibi, E.; Heidari, H. *Electrochim. Acta* **2008**, *53*, 8178.
38. Sheppard, S. A.; Campbell, S. A.; Smith, J. R.; Lloyd, G. W.; Ralph, T. R.; Walsh, F. C. *Analyst* **1998**, *123*, 1923.
39. Laoire, C. O.; Plichta, E.; Hendrickson, M.; Mukerjee, S.; Abraham, K. M. *Electrochim. Acta* **2009**, *54*, 6560.